

Modeling the Microwave Transmissivity of Row Crops

Jeil Park¹, Praveen Gurralla¹, Brian K. Hornbuckle², and Jiming Song¹

¹Department of Electrical and Computer Engineering
Iowa State University, Ames, Iowa 50011-1046, USA
cptpark@iastate.edu, praveeng@iastate.edu, jisong@iastate.edu

²Department of Agronomy
Iowa State University, Ames, Iowa 50011-1051, USA
bkh@iastate.edu

Abstract — We develop a method to model the microwave transmissivity of row crops that explicitly accounts for their periodic nature as well as multiple scattering. We hypothesize that this method could eventually be used to improve satellite retrieval of soil moisture and vegetation optical depth in agricultural regions. The method is characterized by unit cells terminated by periodic boundary conditions and Floquet port excitations solved using commercial software. Individual plants are represented by vertically oriented dielectric cylinders. We calculate canopy transmissivity, reflectivity, and loss in terms of S-parameters. We validate the model with analytical solutions and illustrate the effect of canopy scattering. Our simulation results are consistent with both simulated and measured data published in the literature.

Index Terms — HFSS, scattering, SMOS, SMAP, soil moisture, S-parameters, transmissivity, vegetation optical depth.

I. INTRODUCTION

Both NASA's Soil Moisture Active Passive (SMAP) satellite mission [1] and the European Space Agency's Soil Moisture Ocean Salinity (SMOS) satellite mission [2] use L-band radiometry to estimate soil moisture. Their retrieval algorithms are based on a zeroth-order solution of radiative transfer commonly called the τ - ω model because it uses two parameters, τ and ω , to characterize attenuation and scattering by vegetation [3, 4]. Assessment of SMAP and SMOS performance in croplands reveal that soil moisture retrievals do not satisfy either mission's accuracy goal. It is likely that unrealistic values of τ and ω are part of the problem [5, 6]. The τ - ω model assumes that the vegetation scattering is almost zero at L-band ($f = 1.4$ GHz, $\lambda = 21$ cm). However, when the electrical size of plants becomes comparable with the wavelength, the scattered radiation and its coherent wave interactions generated from all of

the plants are no longer negligible [7, 8].

The τ and ω parameters currently in use are empirical: they have largely been determined by fitting the τ - ω model to observations. There is a need to find more realistic values of τ and ω in order to increase the accuracy of soil moisture estimates in agricultural regions. One approach is to represent the vegetation canopy with models that include vegetation scattering effects. The τ parameter, also called the vegetation optical depth (VOD), is a measure of the transmissivity of vegetation canopy. Experimental observations [9] and theoretical models [10, 11] show that vegetation transmissivity depends on the operation frequency, incidence angle, polarization, and type of vegetation.

We model the vegetation canopy using the FEM solver in HFSS [12], incorporating several key features of croplands in the remote sensing point of view [13, 14]. First, crops are generally planted in regularly-spaced rows, and there are a large number of plants (scatterers) within an L-band satellite footprint (30-40 km). Second, the scattered fields and all the coherent wave interactions need to be considered. Third, the radiation is treated as a plane wave, and the polarization and incident angle should be dealt with. Floquet ports and periodic boundary conditions are used in our proposed approach to realize the features described above. We utilize S-parameters from HFSS directly to calculate the transmissivity of the vegetation canopy. The CPU time and memory requirement for running the simulations are tractable because of restricting the computational domain to a unit cell.

In the following sections, we explain how we model the vegetation canopy in HFSS, and then validate our simulations against analytical results. Finally, we compare our results with published data [9, 10] for a corn and a grass canopy.

II. METHODOLOGY

To model the layer of vegetation, we propose to use

the unit cell comprising the PBC (periodic boundary condition) and two Floquet ports, as shown in Fig. 1. The PBC enforces field periodicity in the x - and y -direction through master/slave boundary pairs, and hence, an infinite array of the 3D structure is created. The Floquet port excites plane waves consisting of an infinite series of TE_z (transverse electric to z , h-pol) and TM_z (transverse magnetic to z , v-pol) Floquet modes [15].

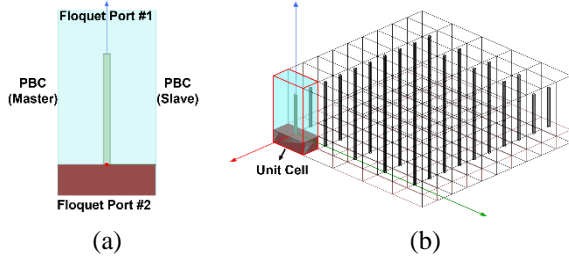


Fig. 1. HFSS modeling of a layer of vegetation: (a) unit cell and (b) infinite array of 3D structure.

A. Plane wave with oblique incidence

The S-parameters as a function of the observation angle can be obtained by defining the phase shift through the slave boundary, as shown in Fig. 2. Formulations in this section follow [16].

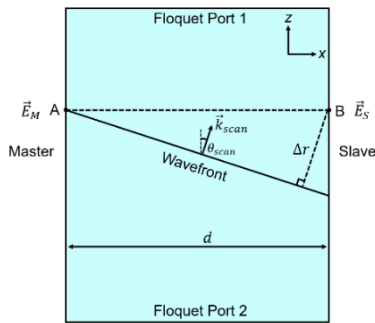


Fig. 2. A pair of master and slave boundaries.

The propagation vector of the radiated wave is given by:

$$\vec{k}_{\text{scan}} = k_0 [\cos \phi_{\text{scan}} \sin \theta_{\text{scan}}, \sin \phi_{\text{scan}} \sin \theta_{\text{scan}}, \cos \theta_{\text{scan}}], \quad (1)$$

where θ_{scan} and ϕ_{scan} are our intended direction in spherical coordinates, $k_0 = \omega \sqrt{\mu_0 \epsilon_0}$ is the free-space wave number, and ϵ_0 and μ_0 are the permittivity and permeability of free space, respectively. The radiated fields at Point A on the master boundary and at Point B on the slave boundary are represented relatively as:

$$\vec{E}_M = \vec{E}_0 \exp[j(\omega t - k_0 r_0)], \quad (2)$$

$$\vec{E}_S = \vec{E}_M \exp(-jk_0 \Delta r), \quad (3)$$

where, ω is the angular frequency. Assuming that the radiated wave is traveling in the xz -plane ($\phi_{\text{scan}} = 0$), as

shown in Fig. 2, the phase shift between Point A and B is obtained by (4), and Eq. (3) can be rewritten as (5):

$$\Delta r = d \sin \theta_{\text{scan}}, \quad (4)$$

$$\vec{E}_S = \vec{E}_M \exp(-jk_0 d \sin \theta_{\text{scan}}). \quad (5)$$

The relationship between the scan angle and the phase shift ($\Delta\Phi$) in degrees through a pair of master/slave boundaries can be expressed as:

$$\Delta\Phi = 360^\circ d \sin \theta_{\text{scan}} / \lambda. \quad (6)$$

Thus, we can excite a plane wave in our intended direction so that transmissivity is computed as a function of the observation angle.

B. TE_z and TM_z Floquet modal fields

The benefit of using the Floquet theory is to be able to derive the electromagnetic fields in terms of Floquet series when solving Maxwell's equations [17]. Also, an arbitrary uniform plane wave can be decomposed into the sum of orthogonal Floquet modal fields (TE_z and TM_z) such that the scattering problem is solved for each polarization. The mathematical expressions for the normalized Floquet modal fields are introduced, and formulations in this subsection follow [17]. The TE_z modal fields, which are referred to as the transverse electric field to z -axis, are generated from the electric vector potential \vec{F} with only z -component. In terms of Floquet harmonics, \vec{F} can be expressed as:

$$\vec{F} = \hat{z} A \exp[-j(k_{xmn} x + k_{ymn} y + k_{zmn} z)], \quad (7)$$

where A is a constant and k_{xmn} , k_{ymn} are the mode wave numbers for the TE_{zmn} Floquet mode. For a rectangular grid, the mode wave numbers for the (m, n) Floquet mode are given by:

$$k_{xmn} = k_{x0} + 2m\pi/a, \quad k_{ymn} = k_{y0} + 2n\pi/b, \quad (8)$$

where a and b are intervals on the xy -plane respectively and analogous to the unit cell size in x - and y -directions in our modeling; m and n are integers varying from $-\infty$ to $+\infty$; k_{x0} and k_{y0} are two constants that determine the progressive phase shift between the nearby cells and are related to the intended direction of radiation (θ_0, ϕ_0). This yields,

$$k_{x0} = k_0 \sin \theta_0 \cos \phi_0, \quad k_{y0} = k_0 \sin \theta_0 \sin \phi_0. \quad (9)$$

Then, the wave number along z -direction is expressed as:

$$k_{zmn}^2 = k^2 - k_{xmn}^2 - k_{ymn}^2, \quad (10)$$

where k is the wave number in the medium. It is noted that the propagation direction of the Floquet modal fields is parallel to the vector \vec{k}_{mn} as follows:

$$\vec{k}_{mn} = \hat{x} k_{xmn} + \hat{y} k_{ymn} + \hat{z} k_{zmn}. \quad (11)$$

The electric fields are derived by solving the relation $\vec{E} = -\nabla \times \vec{F}$. This yields,

$$\vec{E} = jA (\hat{x} k_{ymn} - \hat{y} k_{xmn}) \exp(-j\vec{k} \cdot \vec{r}), \quad (12)$$

where $\vec{r} = x\hat{x} + y\hat{y} + z\hat{z}$. The magnetic fields are also

determined by the Maxwell equation:

$$\nabla \times \vec{E} = -j\omega\mu\vec{H}, \quad (13)$$

as

$$\vec{H} = jAY_{mn}^{\text{TE}} \left(\hat{x}k_{xmn} + \hat{y}k_{ymn} - \hat{z} \frac{k^2 - k_{zmn}^2}{k_{zmn}} \right) \exp(-j\vec{k} \cdot \vec{r}), \quad (14)$$

where Y_{mn}^{TE} is the modal admittance for the TE_{zmn} Floquet mode, and given by:

$$Y_{mn}^{\text{TE}} = k_{zmn} / (\omega\mu). \quad (15)$$

The modal fields are normalized by choosing the constant term A such that the complex power through the Floquet port becomes equal to the complex conjugate of the modal admittance of the TE_{zmn} mode. This yields,

$$\iint_{\text{port}} (\vec{E} \times \vec{H}^*) \cdot \hat{z} \, dx \, dy = Y_{mn}^{\text{TE}*}. \quad (16)$$

Substituting (12) and (14) into (16) yields,

$$A = \frac{1}{j\sqrt{ab}(k^2 - k_{zmn}^2)}. \quad (17)$$

Finally, using (17) in (12), the TE_z modal fields are re-expressed as:

$$\vec{E} = \frac{\hat{x}k_{ymn} - \hat{y}k_{xmn}}{\sqrt{ab}(k^2 - k_{zmn}^2)} \exp(-j\vec{k} \cdot \vec{r}). \quad (18)$$

The TM_z Floquet modal fields can be also solved from the magnetic vector potential \vec{A} , which is expressed as:

$$\vec{A} = \hat{z}B \exp(-j\vec{k} \cdot \vec{r}), \quad (19)$$

where B is a constant. Applying the relation $\vec{H} = \nabla \times \vec{A}$ and the Maxwell equation $\nabla \times \vec{H} = j\omega\epsilon\vec{E}$, the modal admittance is obtained by:

$$Y_{mn}^{\text{TM}} = \omega\epsilon / k_{zmn}. \quad (20)$$

Using a similar procedure as above, the TM_z Floquet modal fields are expressed as:

$$\vec{H} = \frac{(-\hat{x}k_{ymn} + \hat{y}k_{xmn})}{\sqrt{ab}(k^2 - k_{zmn}^2)} \exp(-j\vec{k} \cdot \vec{r}). \quad (21)$$

In the context of our modeling, two factors are considered. First, the unit-cell size ($a \times b$) is determined based on the density of plants, the row spacing, and the average plant spacing. Also, since k_{zmn} is real or imaginary depending on the wavelength and the unit-cell size, it is essential to include all the propagation modes and exclude the evanescent modes [12]. This improves simulation efficiency and interpretation of the S-parameters of interests. Second, we utilize the S-parameter of the zeroth order Floquet mode ($m = n = 0$), which propagates along our intended angle (θ_0, ϕ_0) , as shown in Fig. 3.

C. Generalized scattering matrix

The HFSS solution provides us with S-parameters which are cast in the form of a generalized scattering matrix (GSM), as shown in Fig. 4, where a_{mn} and b_{mn}

are the incident voltage vectors at the two Floquet ports and c_{mn} and d_{mn} are the reflected voltage vectors corresponding to a_{mn} and b_{mn} . The S-matrix interrelates the TE_z (h-pol) and TM_z (v-pol) Floquet modes, where S_{11} and S_{22} are the reflection coefficients, and S_{12} and S_{21} are the transmission coefficients. Also, the coupling effect with two different polarizations is given in the GSM.

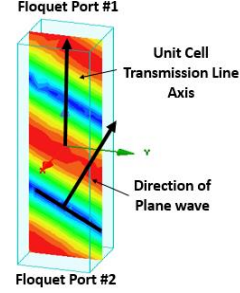


Fig. 3. Field overlays of the zeroth order Floquet mode with scan angle $(\theta_0, \phi_0) = (40^\circ, 90^\circ)$.

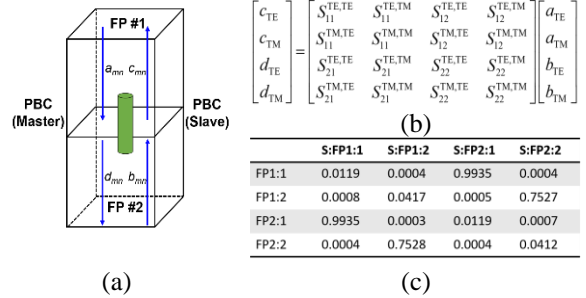


Fig. 4. (a) Configuration of the unit cell. (b) Generalized scattering matrix. (c) HFSS solution.

Therefore, we obtain the S-parameters for the vegetation canopy case consisting of an infinite number of 3D structures which represent the plants that make up the canopy of a row crop. The transmissivity, γ , of the vegetation canopy is computed as:

$$\gamma_u = \left[|S_{12}^{\text{hh}}|^2 + |S_{12}^{\text{hv}}|^2 + |S_{12}^{\text{vh}}|^2 + |S_{12}^{\text{vv}}|^2 \right] / 2, \quad (22)$$

$$\gamma_v = |S_{12}^{\text{vv}}|^2, \quad \gamma_h = |S_{12}^{\text{hh}}|^2, \quad (23)$$

where the superscripts and subscripts u, v , and h denote the unpolarized, vertically-polarized (v-pol), and horizontally-polarized (h-pol) transmissivities, respectively, and the denominator 2 is the total excitation power of two polarizations from Port 2. In detail, we assign the same power of 1 W to each TE_{00} and TM_{00} Floquet mode.

III. VALIDATION AND SIMULATIONS

Our method is validated with analytical solutions and then compared with results from [9-10, 18].

A. 2-layer and 3-layer case

A 2-layer case (air and soil) is simulated to compute the Fresnel reflectivity and transmissivity as shown in Fig. 5. The analytical solutions for $|S_{11}|^2$ and $|S_{21}|^2$ when the wave propagates from Port 1 to Port 2 are computed as:

$$|S_{11}|^2 = |R_{12}|^2 \quad \text{for v-pol and h-pol,} \quad (24)$$

$$|S_{21}|^2 = \begin{cases} e^{-2\alpha_{2z}d} \frac{\text{Im}[\gamma_{2z}]}{\text{Im}[\gamma_{1z}]} |T_{21}^h|^2 & \text{for h-pol,} \\ e^{-2\alpha_{2z}d} \frac{\text{Im}[\gamma_{2z}/\epsilon_2]}{\text{Im}[\gamma_{1z}/\epsilon_1]} |T_{21}^v|^2 & \text{for v-pol,} \end{cases} \quad (25)$$

where R is the Fresnel reflection coefficient, T is the transmission coefficient, subscripts 1 and 2 denote air and soil respectively, $\gamma (= \alpha + j\beta)$ is the complex propagation constant consisting of the attenuation constant (α , Np/m) and the phase constant (β , rad/m), d is the soil depth, and the soil attenuation constant α_{2z} along the z -direction is calculated by:

$$\begin{aligned} \gamma_i &= \alpha_i + j\beta_i = \sqrt{-\omega^2 \tilde{\epsilon}_i \mu_0}, \quad i=1,2 \\ \gamma_{iz} &= \alpha_{iz} + j\beta_{iz} = \sqrt{\gamma_i^2 - \gamma_{ix}^2}, \\ \gamma_{2x} &= \gamma_{1x} = jk_1 \sin \theta_1, \end{aligned} \quad (26)$$

where $\tilde{\epsilon}_i$ is the complex permittivity.

The analytical solutions for $|S_{22}|^2$ and $|S_{12}|^2$ when the waves propagate from Port 2 to 1 are computed as:

$$|S_{22}|^2 = e^{-4\alpha_{2z}d} |R_{21}|^2 \quad \text{for v-pol and h-pol,} \quad (27)$$

$$|S_{12}|^2 = \begin{cases} e^{-2\alpha_{2z}d} e^{-2\alpha_{1z}h} \frac{\text{Im}[\gamma_{1z}]}{\text{Im}[\gamma_{2z}]} |T_{12}^h|^2 & \text{for h-pol,} \\ e^{-2\alpha_{2z}d} e^{-2\alpha_{1z}h} \frac{\text{Im}[\gamma_{1z}/\tilde{\epsilon}_1]}{\text{Im}[\gamma_{2z}/\tilde{\epsilon}_2]} |T_{12}^v|^2 & \text{for v-pol,} \end{cases} \quad (28)$$

where h is the height of air layer, and the attenuation constants for each layer are calculated using (26) with $\gamma_{2x}^2 = \gamma_{1x}^2 = -\omega^2 \text{Re}[\tilde{\epsilon}_2] \mu_0 \sin^2 \theta_1$. Figures 6 and 7 show that the reflected or transmitted power can be computed accurately using our method.

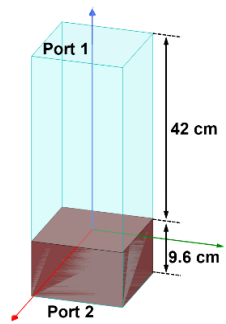
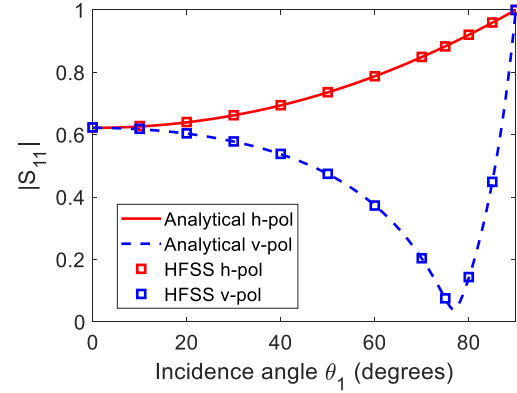
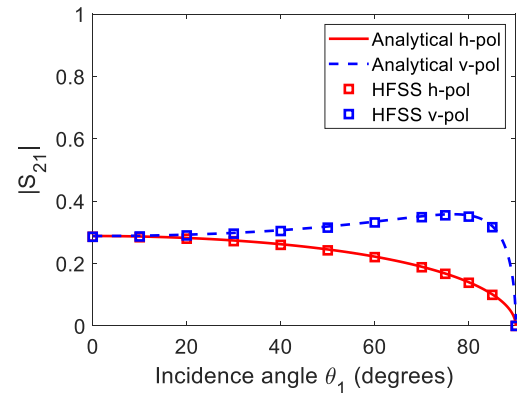


Fig. 5. HFSS model for the 2-layer case (soil and air) where the soil relative complex permittivity $\tilde{\epsilon}_{r,\text{soil}} = 18 - j3$ at the operation frequency of 1.41 GHz.



(a) Reflection coefficient



(b) Transmission coefficient

Fig. 6. Reflection coefficient $|S_{11}|$ and transmission coefficient $|S_{21}|$ of the 0th-order Floquet mode when the wave propagates downward in Fig. 5.

A 3-layer case where the vegetation canopy is added between the soil layer and the air layer in the unit cell as shown in Fig. 8 is also simulated to illustrate the effect of scattering.

In the homogeneous layer case, the vegetation canopy is treated as a homogeneous medium with an effective permittivity. The effective permittivity $\tilde{\epsilon}_{\text{eff}} (= 1.98 - j0.35)$ is obtained by:

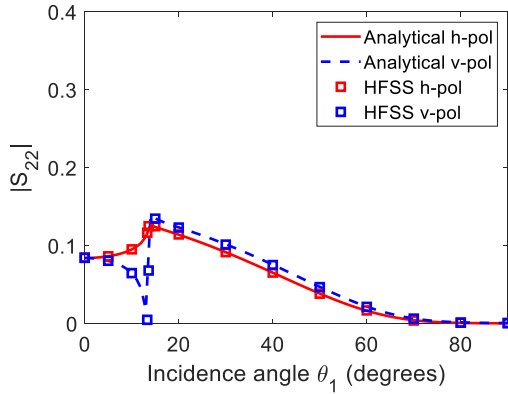
$$\tilde{\epsilon}_{\text{eff}} = \frac{V_{\text{air}}}{V_{\text{total}}} \epsilon_{\text{air}} + \frac{V_{\text{stem}}}{V_{\text{total}}} \tilde{\epsilon}_{\text{stem}}, \quad (29)$$

where the dimension of cylinder is 1.5 cm in radius and 30 cm in height, the volume fraction of cylinder (stem) is 7.1% ($V_{\text{total}} = 3 \times 10^{-3} \text{ m}^3$, $V_{\text{air}} = 2.788 \times 10^{-3} \text{ m}^3$ and $V_{\text{stem}} = 2.12 \times 10^{-4} \text{ m}^3$), and the cylinder's relative permittivity is $\tilde{\epsilon}_{\text{stem}} = 15 - j15$ [10]. The analytical solution for $|S_{11}|$ in the homogeneous layer case is computed as [19]:

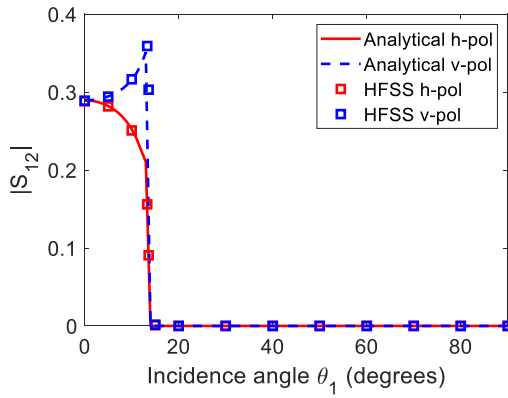
$$R^{\text{total}} = \frac{R_{12} + R_{23} e^{-2\gamma_{2z}h}}{1 + R_{12}R_{23} e^{-2\gamma_{2z}h}}, \quad (30)$$

where R^{total} is the total reflection coefficient of the wave propagating upward in medium 1 (air), R_{12} and R_{23} are

the half-space reflection coefficients at each interface, and h is the vegetation canopy’s height.



(a) Reflection coefficient



(b) Transmission coefficient

Fig. 7. Reflection coefficient $|S_{22}|$ and transmission coefficient $|S_{12}|$ of the 0th-order Floquet mode when the wave propagates upward in Fig. 5.

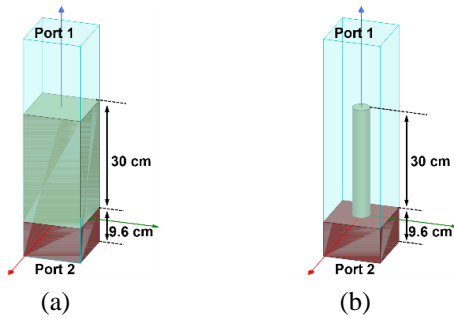
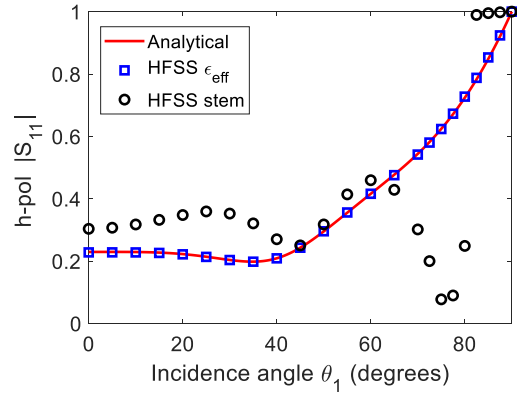


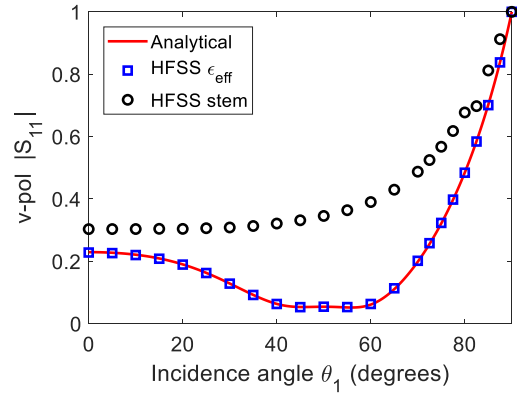
Fig. 8. HFSS model for the 3-layer case when the wave propagates downward from Port 1 to Port 2: (left) the homogeneous layer case (right) and the stem case.

In the stem case, where the vegetation canopy consists of an infinite number of finite-length cylinders, the incident wave from Port 1 induces currents on the

cylinders, which generate the scattered radiation. Therefore, $|S_{11}|$ in this case accounts for vegetation scattering and coherency induced by scattering between the stem and the soil surface. Fig. 9 shows that first, the results of the two approaches (analytical solution and homogeneous layer case) are in good agreement. Second, the reflectivity simulated using the homogenous layer and effective permittivity based on the volume fraction of air to stem is not the same as the reflectivity of the more realistic vegetation canopy (stem).



(a) H-pol



(b) V-pol

Fig. 9. Reflection coefficient $|S_{11}|$ of the 0th-order Floquet mode for each polarization when the wave propagates downward in Fig. 8.

B. Grass canopy

Two cases, as shown in Fig. 10 are compared with each other: the randomly distributed case was studied using the NMM3D (numerical Maxwell model in 3D simulations) [10], and the periodically distributed case is simulated in this work using the HFSS model.

Parameters used in these two cases are as follows: the cylinder has a radius of 1 mm, length of 30 cm, and relative complex permittivity of $30.7 - j5.5$, the operation frequency is 5.4 GHz (C-band), the density is 2122 cylinders per m^2 , and the incidence angle is 40° .

These parameters represent the water column density of a $1\text{ kg} \cdot \text{m}^{-2}$ grass canopy. The transmissivity of the grass canopy is computed by using the HFSS model, as shown in Fig. 11.

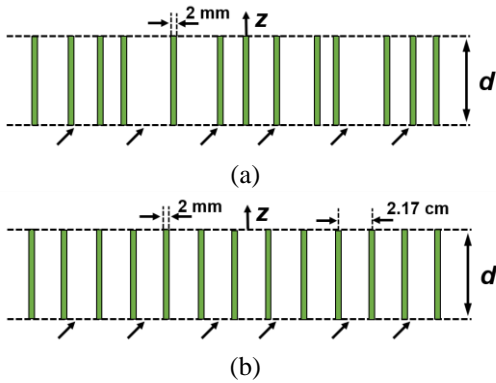


Fig. 10. One layer consisting of long and thin cylinders (a) randomly distributed [10] and (b) periodically distributed with a spacing of 2.17 cm between cylinders in both directions.

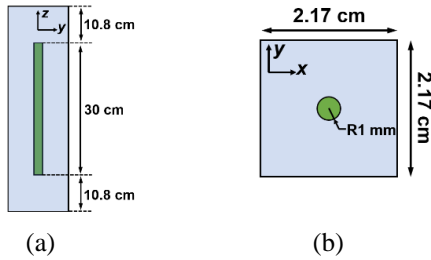


Fig. 11. Schematic of HFSS model for the grass canopy: (a) front view and (b) top view.

Table 1 shows the comparison between our method and the NMM3D for the cases of Fig. 10. The transmissivity found using our method for the periodically distributed case (0.78) is similar to, but not the same as, the transmissivity found using the NMM3D for the randomly distributed case (0.70). However, the standard deviation of multiple realizations of the randomly-distributed case is 0.2. We hypothesize that more coherent wave interactions take place among the vegetation scatters in the periodically distributed case than in the randomly distributed case.

For the model in Fig. 10 (b), we also compute the transmissivity for each polarization as a function of frequency. Figure 12 shows that the transmissivity decreases as the frequency increases. In other words, the grass vegetation canopy is increasingly opaque as the wavelength becomes shorter. Also, the loss for the

vertical polarization is greater than the horizontal polarization since the vegetation canopy consists of vertically-oriented stems.

Table 1: Transmissivity at an incident angle 40° for the grass canopy. $\tau = -\cos\theta \ln\gamma$

Methodology / Distribution	HFSS / Periodically	NMM3D / Sparsely [10]
Transmissivity (γ)	0.78	0.70
VOD (τ)	0.64	0.89

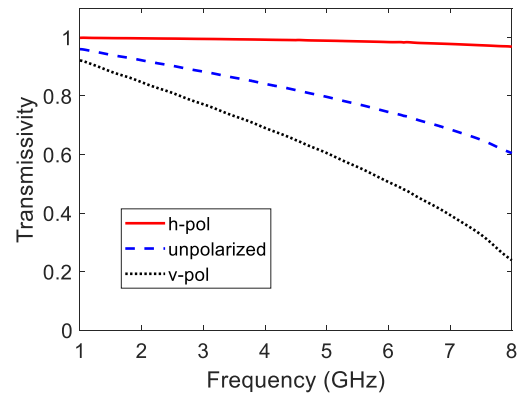


Fig. 12. Transmissivity at an incident angle 40° for the grass canopy as a function of frequency (f : 1 – 8 GHz, λ : 30 cm – 3.75 cm).

C. Corn canopy

Experimental observations for the vegetation canopy consisting of vertically oriented stalks were conducted in [9]. Parameters are as follows: row spacing is 76 cm, average plant spacing is 19.8 cm, average plant height is 2.7 m with average diameter 1.7 cm, relative complex permittivity is $16.9 - j5.6$, and the operation frequency is 1.62 GHz. Based on these parameters, the HFSS model is created, as shown in Fig. 13.

The radiation excited from the Floquet port is set up to propagate at $\theta = 20^\circ, 40^\circ, 60^\circ$, and $\phi = 90^\circ$ in accordance with the measurement set-up in the literature. The loss L in dB for the corn canopy can be computed as:

$$L_v = -20 \log(|S_{21}^{vv}|), \quad L_h = -20 \log(|S_{21}^{hh}|). \quad (31)$$

Table 2 shows the comparison between our method and the experimental observation. First, our simulation results are in the range of the measured data. Second, h-pol loss is less than v-pol loss. Also, it is observed that the loss increases as the incidence angle increases for the v-pol, whereas h-pol does not exhibit the same pattern. We hypothesize this is because the stem diameter of 1.7 cm is small compared to the wavelength of 18.5 cm.

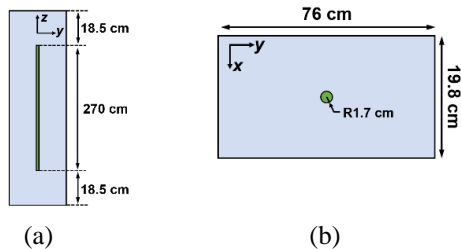


Fig. 13. Schematic of HFSS model for the corn canopy: (a) front view and (b) top view.

Table 2: Loss for the corn canopy where the experiment result presents the mean value of the measured loss and the $\pm 25\%$ confidence interval

Incident angle	V-pol loss	
	Experiment [9]	HFSS
20°	1.4 dB (1.0–1.7 dB)	1.0 dB
40°	5.3 dB (3.3–9.2 dB)	6.3 dB
60°	8.5 dB (6.5–11.9 dB)	9.0 dB

Incident angle	H-pol loss	
	Experiment [9]	HFSS
20°	0.7 dB (0.2–1.3 dB)	0.4 dB
40°	0.7 dB (0–1.7 dB)	0.2 dB
60°	1.2 dB (0.3–2.0 dB)	0.3 dB

IV. CONCLUSION

We used a method consisting of Floquet ports and periodic boundary conditions to model a layer of vegetation where an infinite number of vegetation elements (plants) are arrayed in the x - and y -direction like in a row crop. The scattered fields and its coherent interactions are considered by solving Maxwell's equations directly using HFSS, and the transmissivity is computed by utilizing the S -parameters. The simulation results from our proposed model and the NMM3D model for a grass canopy, as well as experimental measurements of a corn canopy, are similar. Some of the differences are likely due to the periodicity enforced in our method, which limits the distribution of vegetation elements within rows, when in reality the in-row spacing between elements is somewhat random. Our method could be used to find the transmissivity of different crops. In the future, we plan to enhance our plant models by adding leaf-like structures to the cylinders (stalks). We hope our method can eventually be used to find more realistic values of the parameters of the $\tau - \omega$ model used by SMOS and SMAP and consequently improved retrievals of soil moisture and VOD in croplands.

REFERENCES

- [1] D. Entekhabi, E. G. Njoku, P. E. O'Neill, K. H. Kellogg, W. T. Crow, W. N. Edelstein, J. K. Entin, S. D. Goodman, T. J. Jackson, J. Johnson, J. Kimball, J. R. Piepmeier, R. D. Koster, N. Martin, K. C. McDonald, M. Moghaddam, S. Moran, R. Reichle, J. C. Shi, M. W. Spencer, S. W. Thurman, L. Tsang, and J. Van Zyl, "The soil moisture active passive (SMAP) mission," *Proceedings of the IEEE*, vol. 98, no. 5, pp. 704-716, May 2010.
- [2] Y. H. Kerr, P. Waldteufel, J.-P. Wigneron, S. Delwart, F. Cabot, J. Boutin, M.-J. Escorihuela, J. Font, N. Reul, C. Gruhier, S. N. Juglea, M. R. Drinkwater, A. Hahne, M. Martín-Neira, and S. Mecklenburg, "The SMOS mission: New tool for monitoring key elements of the global water cycle," *Proceedings of the IEEE*, vol. 98, no. 5, pp. 666-687, May 2010.
- [3] J.-P. Wigneron, Y. Kerr, P. Waldteufel, K. Saleh, M.-J. Escorihuela, P. Richaume, P. Ferrazzoli, P. de Rosnay, R. Gurney, J.-C. Calvet, J.P. Grant, M. Guglielmetti, B. Hornbuckle, C. Mätzler, T. Pellarin, and M. Schwank, "L-band microwave emission of the biosphere (L-MEB) model: Description and calibration against experimental data sets over crop fields," *Remote Sensing of Environment*, vol. 107, no. 4, pp. 639-655, 2007.
- [4] P. O'Neill, S. Chan, E. Njoku, T. Jackson, and R. Bindlish, "Algorithm theoretical basis document level 2 & 3 soil moisture (passive) data products; revision B," *Jet Propulsion Lab., California Inst. Technol.: Pasadena, CA, USA*, 2017.
- [5] V. A. Walker, B. K. Hornbuckle and M. H. Cosh, "A five-year evaluation of SMOS level 2 soil moisture in the corn belt of the United States," *IEEE Journal of Selected Topics in Applied Earth Observations and Remote Sensing*, vol. 11, no. 12, pp. 4664-4675, Dec. 2018.
- [6] V. A. Walker, B. K. Hornbuckle, M. H. Cosh, and J. H. Prueger, "Seasonal evaluation of SMAP soil moisture in the U.S. corn belt," *Remote Sensing*, vol. 11, no. 21, pp. 5-7, 2019.
- [7] M. Kurum, "Quantifying scattering albedo in microwave emission of vegetated terrain," *Remote Sensing of Environment*, vol. 129, pp. 66-74, 2013.
- [8] B. K. Hornbuckle and T. L. Rowlandson, "Evaluating the first-order tau-omega model of terrestrial microwave emission," *IEEE International Geoscience and Remote Sensing Symposium (IGARSS)*, pp. 193-196, July 2008.
- [9] F. T. Ulaby, A. Tavakoli, and B. A. Thomas, "Microwave propagation constant for a vegetation canopy with vertical stalks," *IEEE Transactions on*

Geoscience and Remote Sensing, vol. 25, no. 6, pp. 714-725, Nov. 1987.

- [10] H. Huang, L. Tsang, E. G. Njoku, and A. Colliander, "A new vegetation model based on numerical 3D solutions of Maxwell equations," *IEEE International Geoscience and Remote Sensing Symposium (IGARSS)*, pp. 2903-2906, July 2017.
- [11] A. Colliander, E. G. Njoku, H. Huang, and L. Tsang, "Soil moisture retrieval using full wave simulations of 3-D Maxwell equations for compensating vegetation effects," *IEEE International Geoscience and Remote Sensing Symposium (IGARSS)*, pp. 1418-1421, July 2018.
- [12] HFSS documentation: Floquet Ports, Ansoft Corporation, Canonsburg, PA, USA, 2016.
- [13] M. Malajner and D. Gleich, "Soil moisture estimation using UWB," *Applied Computational Electromagnetics Society Conference*, pp. 298-299, Honolulu, HI, USA, Mar. 2016.
- [14] K. P. Prokopidis and T. D. Tsiboukis, "Modeling of ground-penetrating radar for detecting buried objects in dispersive soils," *Applied Computational Electromagnetics Society Journal*, vol. 22, no. 2, pp. 287-294, July 2007.
- [15] HFSS Workshop 9-1: Unit cell analysis (infinite array), Ansoft Corporation, Canonsburg, PA, USA, 2015.
- [16] S. N. Makarov and A. Puzella, "Scan impedance for an infinite dipole array: Hansen's formulas compared with Ansoft HFSS simulations [EM programmer's notebook]," *IEEE Antennas and Propagation Magazine*, vol. 49, no. 4, pp. 143-156, Aug. 2007.
- [17] A. K. Bhattacharyya, *Phased Array Antennas: Floquet Analysis, Synthesis, BFNs and Active Array Systems*, 1st ed. Wiley-Interscience, 2006.
- [18] C. A. Balanis, *Advanced Engineering Electromagnetics*, 2nd ed., pp. 188-208, John Wiley & Sons, 2012.
- [19] W. C. Chew, *Waves and Fields in Inhomogeneous Media*, 1st ed., pp. 49-53, Wiley-IEEE Press, 1995.



Jeil Park was born in Seoul, Korea. He received the B.E. degree from Korea Military Academy, Korea, in 2011 and the M.S. degree in Electrical Engineering from Iowa State University, USA, in 2020. He is servicing active duty in the ROK army. His research interests focus on modeling and simulations of vegetation canopy and scattering parameter analysis.



Praveen Gurralla received the B.Tech degree from Indian Institute of Technology Madras in 2014, and the Ph.D. degree from Iowa State University in 2020, both in electrical engineering. He is currently an EMI characterization engineer at Micron Technology, Inc. His research interests include computational modeling of ultrasonic and eddy current NDE inspections, fast-multipole boundary element methods, and capacitance tomography.



Brian K. Hornbuckle received the Ph.D. degree in Electrical Engineering and Atmospheric Science from the University of Michigan in 2003. He is presently a Professor in the Department of Agronomy at Iowa State University. Hornbuckle's research goal is to use satellite microwave remote sensing to monitor the movement of water among the soil, vegetation, and atmosphere in agricultural regions. He is a member of the IEEE Geoscience and Remote Sensing Society, the American Geophysical Union, the Soil Science Society of America, and the American Society of Agronomy.



Jiming Song received Ph.D. degree in Electrical Engineering from Michigan State University in 1993. From 1993 to 2000, he worked as a Postdoctoral Research Associate, a Research Scientist and Visiting Assistant Professor at the University of Illinois at Urbana-Champaign. From 1996 to 2000, he worked part-time as a Research Scientist at SAIC-DEMACO. Song was the principal author of the Fast Illinois Solver Code (FISC). He was a Principal Staff Engineer/Scientist at Semiconductor Products Sector of Motorola in Tempe, Arizona before he joined Department of Electrical and Computer Engineering at Iowa State University as an Assistant Professor in 2002.

Song currently is a Professor at Iowa State University's Department of Electrical and Computer Engineering. His research has dealt with modeling and simulations of electromagnetic, acoustic and elastic wave propagation, scattering, and non-destructive evaluation, electromagnetic wave propagation in metamaterials and periodic structures and applications, interconnects on lossy silicon and radio frequency components, antenna radiation and electromagnetic wave scattering using fast algorithms, and transient electromagnetic fields. He received the NSF Career Award in 2006 and is an IEEE Fellow and ACES Fellow.